SUPPLEMENTAL INFORMATION

SUPPLEMENTAL FIGURES AND FIGURE LEGENDS

Fig. S1 Kibe et al.

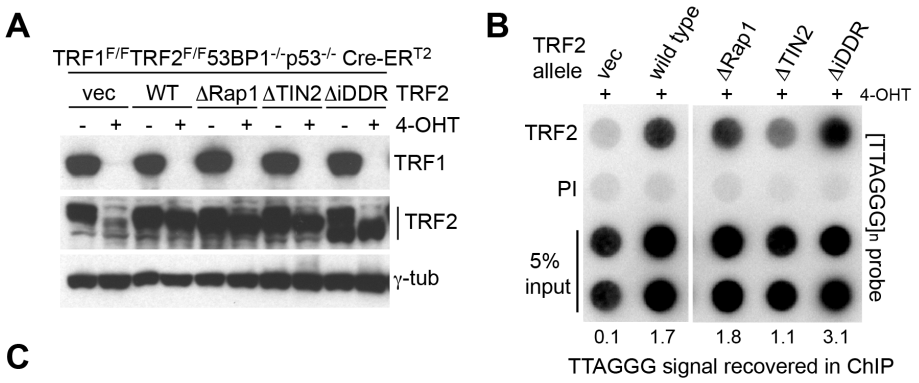

C

TRF1F/FTRF2F/F53BP1-/-p53-/- Cre-ERT2 MEFs + 4-OHT (chromosome ends scored)			chromosome-type fusions (%)	chromatid-type fusions (%)	sister telomere associations (%)	fragile telomeres (%)
vec	(10016)	*	11.1 (12.3, 6.1, 14.9)	1.6	7.8	11.7
TRF2	(6380)		3.3	1.5	4.0	8.5
TRF2ΔRap1	(6984)		2.8	2.2	3.9	9.4
TRF2ΔTIN2	(11188)		3.6 (3.5, 4.2, 3.2)	1.2	7.2	10.2
TRF2ΔiDDR	(6604)		2.0	0.4	21.3	8.1

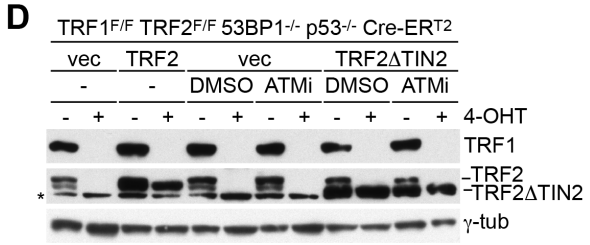

Supplemental Figure S1. Related to Fig. 1. Characterization of TRF2-complemented TRF1/TRF2/53BP1 TKO cells.
(A) Immunoblot to verify the deletion TRF1 and TRF2. g-tubulin is shown as a loading control. Wild type TRF2 or the indicated mutants were over-expressed TRF1$^{F/F}$TRF2$^{F/F}$53BP1$^{-/-}$p53$^{-/-}$ MEFs and analyzed at 96 h after the treatment with 4-OHT.
(B) Telomeric chromatin immunoprecipitation (ChIP) assay for the presence of TRF2 alleles at telomeres. Time point as in (A). Values below panels present average percent telomeric DNA in the ChIPs in two independent experiments.
(C) Table summarizing the telomere phenotypes observed in TRF1$^{F/F}$TRF2$^{F/F}$53BP1$^{-/-}$ p53$^{-/-}$ MEFs expressing the indicated TRF2 mutants after treatment with 4-OHT. For

vector and TRF2ΔTIN2, values represent averages of three independent experiments (at 92-96 h time point). For others, values are averages from two independent experiments (at 96 h time point). *, $P < 0.05$ (two-tailed Student's *t* test).
(D) Immunoblot showing unaltered expression of wild type TRF2 and TRF2ΔTIN2 after ATM inhibition. MEF cells were analyzed at 96 h after 4-OHT. Asterisk indicates a non-specific band and γ-tubulin is used as a loading control.

Fig. S2. Kibe et al.

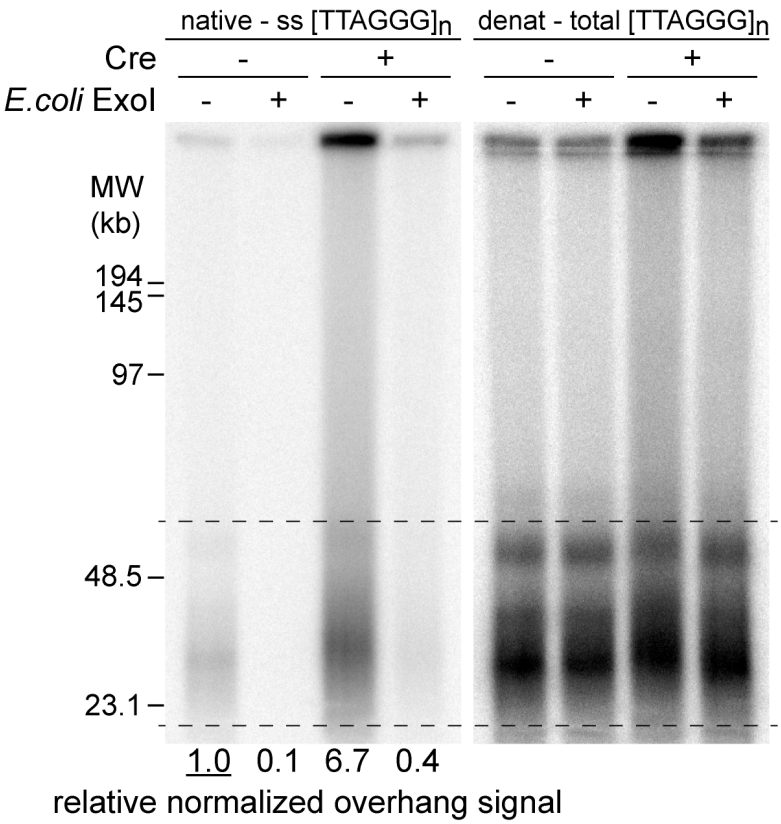

Supplemental Figure S2. Related to Fig. 2. Excess ss telomeric DNA in the TPP1/53BP1 DKO cells derives from extended 3' overhangs.
In-gel overhang assay on DNA from TPP1$^{F/F}$53BP1$^{-/-}$ cells at 96 h after Cre infection. The DNA was treated with *E.coli* 3' Exonuclease I (ExoI) as indicated prior to *Mbo*I digestion. The relative normalized overhang value obtained for cells without Cre and ExoI treatment was set as 1.0. Note that deletion of TPP1 results in telomeric restriction fragments that migrate slightly slower and this reduced migration is negated by 3' exonuclease digestion. This shift to higher apparent MW of the bulk telomeres suggests that the aberrant 5' end resection takes place at most telomeres.

Fig. S3. Kibe et al.

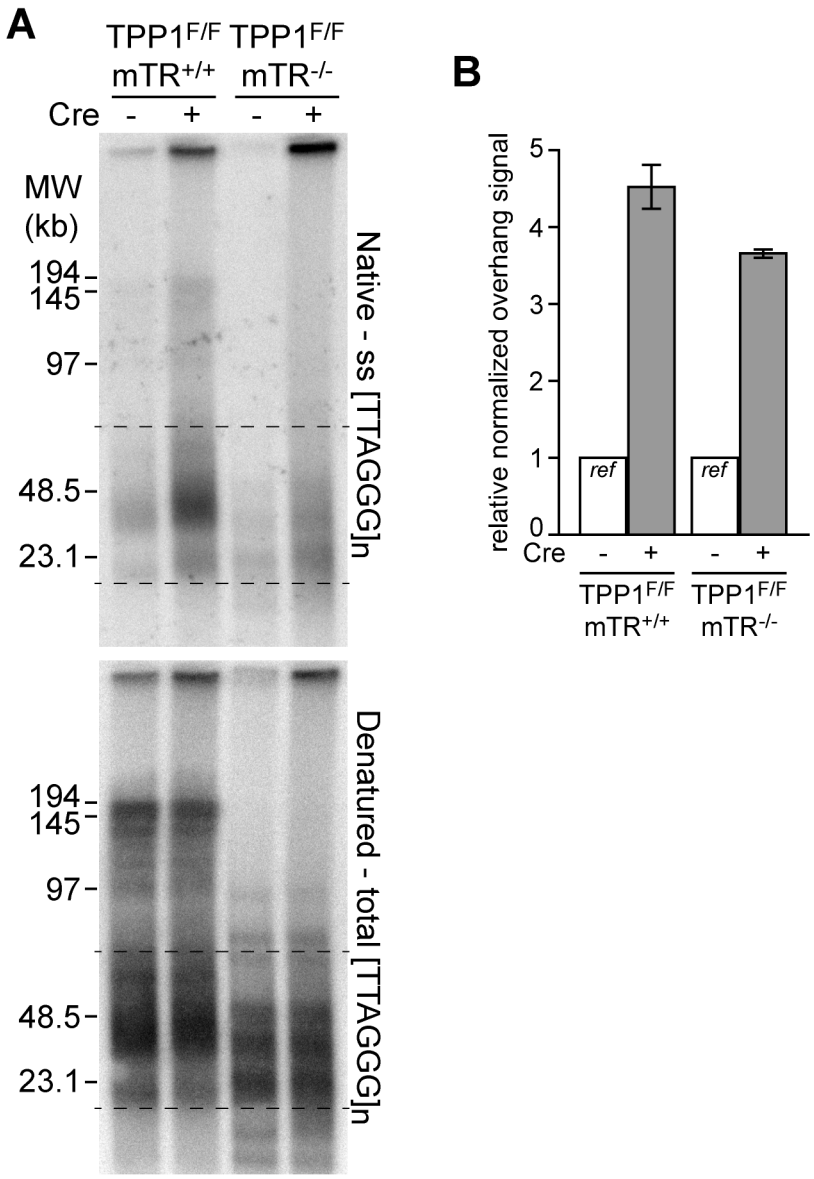

Supplemental Figure S3. Related to Fig. 2. Absence of telomerase does not affect the overhang signal in TPP1 KO cells.
(A) In-gel overhang assay of TPP1$^{F/F}$ and TPP1$^{F/F}$mTR$^{-/-}$ MEFs at 96 h after Cre treatment.
(B) Quantification of the overhang signals from two independent experiments as in (A). Graph shows means ± SEMs.

Fig. S4. Kibe et al.

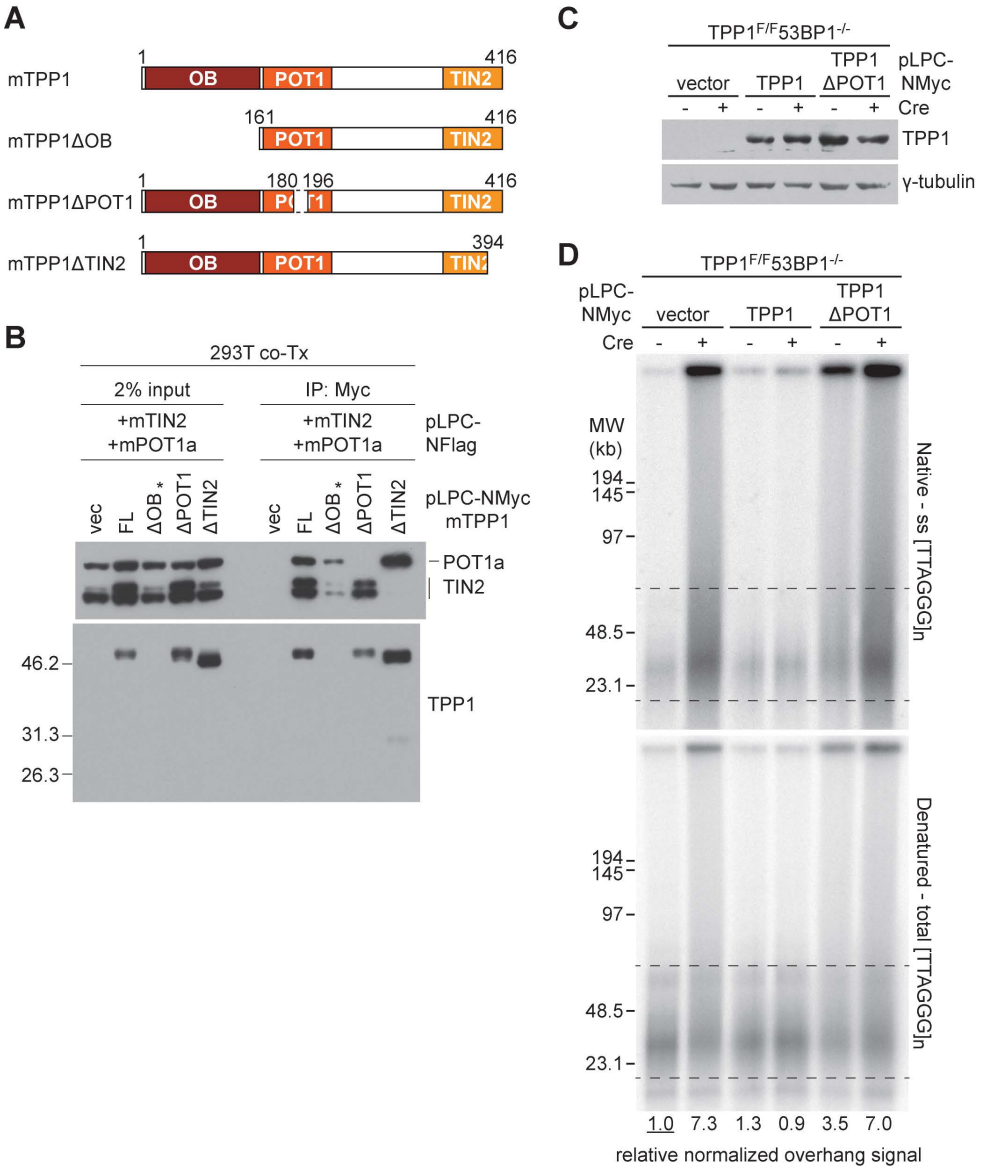

Supplemental Figure S4. Related to Fig. 2. Telomere hyper-resection in TPP1/53BP1-deficient cells is due to POT1a/b loss.

(A) The schematic of TPP1 mutants.

(B) Verification of the loss of TPP1-POT1a interaction in TPP1ΔPOT1. Myc-mTPP1 wt and mutants, Flag-mPOT1a, and Flag-mTIN2 were co-expressed in 293T cells. Myc-mTPP1 wt and mutants were immunoprecipitated with Myc antibody. Interactions with POT1a and TIN2 were detected with Flag immunoblotting. TPP1ΔOB was included in the experiment but is not relevant to this study.

(C) Expression of exogenous wt TPP1 and TPP1ΔPOT1 in TPP1$^{F/F}$53BP1$^{-/-}$ MEFs. Cells were analyzed at 96 h after Cre. The endogenous TPP1 could not be detected in the experiment. γ-tubulin is shown as a loading control.

(D) In-gel overhang assay of TPP1$^{F/F}$53BP1$^{-/-}$ cells expressed TPP1 wt or TPP1ΔPOT1 as in (C). TPP1 wt, but not TPP1ΔPOT1 mutant repressed telomere hyper-resection in TPP1/53BP1 DKO cells.

Fig. S5. Kibe et al.

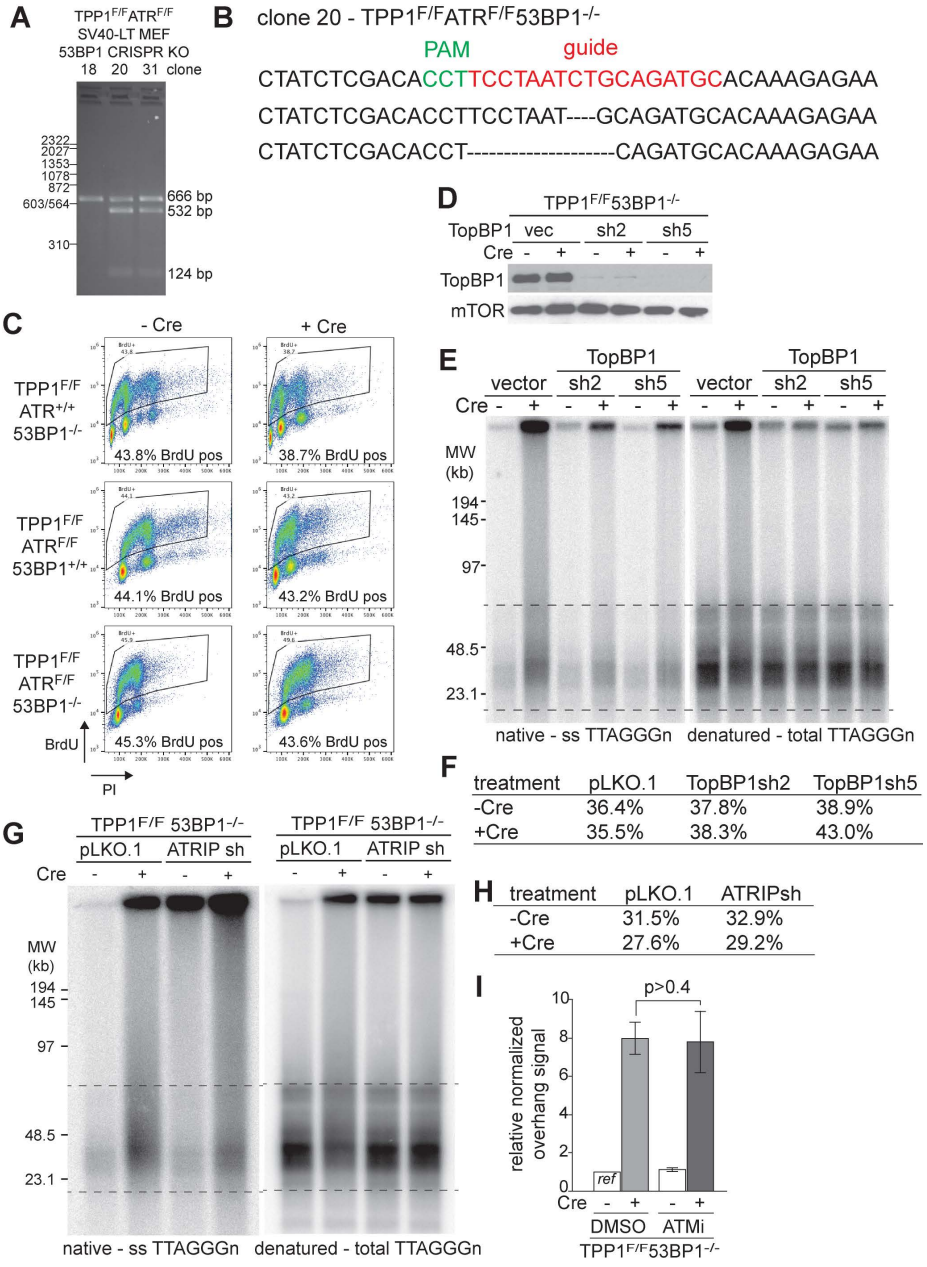

Supplemental Figure S5. Related to Fig. 4. Inhibition of ATR signaling and resection in absence of TPP1.
(A) T7 endonuclease1 assay showing 53BP1 gene modification in TPP1$^{F/F}$ATR$^{F/F}$ clones.
(B) DNA sequence of CRSPR/Cas9 53BP1 targeting region. Guide RNA (red) and PAM (green) are shown in the reference sequence.
(C) BrdU-FACS profile of the indicated cells. 10 μM BrdU was incorporated for 2 h. x axis, propidium iodide; y axis, BrdU prior to harvest cells at 96 h after Cre.
(D) Verification of TopBP1 knockdown by lentiviral shRNAs in TPP1$^{F/F}$53BP1$^{-/-}$ cells. Cells were analyzed at 96 h after Cre treatment. mTOR is shown as a loading control.

(E) Example of in-gel overhang assay of TopBP1 depleted TPP1/53BP1 DKO cells as in (D).
(F, and H) Quantification of the BrdU positive cells. $TPP1^{F/F}53BP1^{-/-}$ cells with TopBP1 or ATRIP shRNAs. 10 μM BrdU was incorporated for 2 h prior to harvest cells at 96 h after Cre.
(I) Hyper-resection in $TPP1^{F/F}53BP1^{-/-}$ MEF cells occurred independently of ATM. Cells were treated with 2.5 μM ATM inhibitor for 108 h before analysis at 96 h post-Cre infection. Data represent means ± SD from three independent experiments.

Fig. S6. Kibe et al.

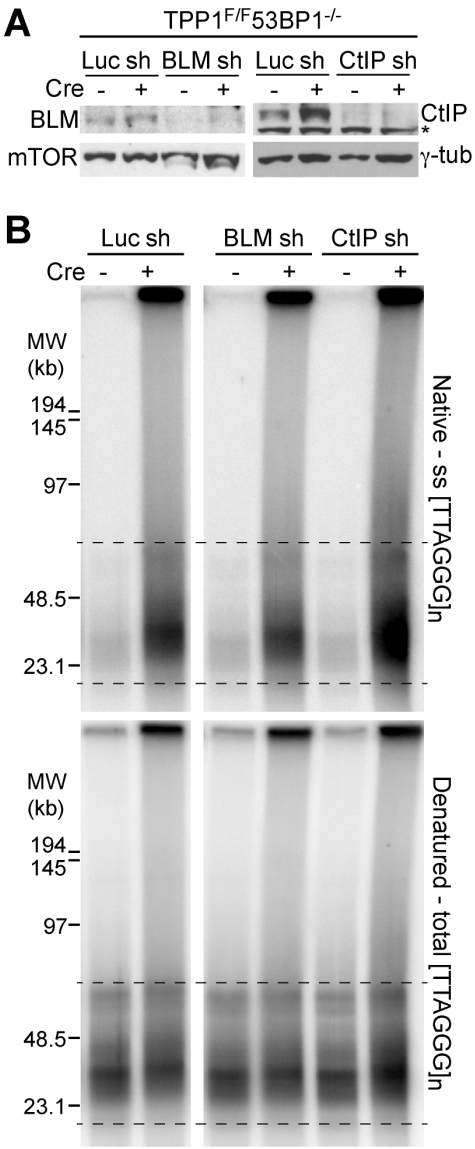

Supplemental Figure S6. Related to Fig.5
(A) Immunoblotting for knockdown of BLM and CtIP in TPP1$^{F/F}$53BP1$^{-/-}$ cells treated with the indicated shRNAs (+Cre: 96 h after Cre). mTOR and γ-tubulin are used as loading controls; non-specific bands are indicated with asterisks.
(B) Example of in-gel overhang assay on the TPP1$^{F/F}$53BP1$^{-/-}$ MEFs treated with CtIP or BLM shRNAs at 96 h after Cre treatment.